Ensembles of Nanoparticles and Fluorescent Molecules

Filip Teodor Corlan

June 2025

1 Introduction

Plasmonic nanoparticles (NPs) offer a powerful route to engineer light–matter interaction at the nanoscale. By concentrating electromagnetic energy into sub-wavelength volumes, they can enhance radiative decay rates, open new non-radiative channels, and thereby reshape the quantum yield (QY) of nearby fluorophores[1,2,3]. Such control is pivotal for applications ranging from single-molecule sensing[4] and super-resolution microscopy[5] to brighter solid-state light sources[6] and deterministic single-photon emitters[7,8].

Gold nanospheres and nanorods constitute two experimentally accessible and well-characterized platforms[9,3] with very different near-field landscapes. The high symmetry of a sphere leads to isotropic field confinement, whereas a nanorod supports a longitudinal and a transverse plasmon mode with intensely concentrated fields at its tips[7]. Although the single-emitter response of each geometry is well understood, it remains unclear how these near-field landscapes influence the ensemble-averaged QY for mobile, randomly oriented chromophores at realistic number densities and with broad distributions of emitter–NP separations.

To address this gap, we combine surface-integral-equation (SIE) electrodynamic modeling, whose efficiency stems from discretizing only particle surfaces[10,11], with a parallel C++/Python Monte Carlo engine that samples realistic ensembles of molecule–nanoparticle configurations. From the SIE solver we extract distance- and orientation-dependent radiative-enhancement (F_{rad}) and quenching (F_q) tensors. The Monte Carlo simulation then links these tensors to statistically distributed chromophores, yielding the mean QY enhancement for arbitrary intrinsic QY values without further electromagnetic calculations.

Understanding the possible range of QY enhancement for such systems and the conditions at which they appear will help with the design and optimization of brighter quantum-dot LEDs, where a modest rise in the mean quantum yield translates directly into higher device efficiency.[6]

2 Methodology

The simulation is divided into two parts. In the first, we compute the radiative enhancement tensor F_{rad} and the quenching tensor F_q for the molecule at selected points in space using a surface integral equation (SIE) approach. In this study, we focus solely on the change in the emission process of the molecules. The analysis remains the same, regardless of the excitation method, such as electrical excitation or optical excitation at a frequency far from the resonant plasmon frequency.

In the second part we perform a Python Monte Carlo simulation, specifying the domain, the concentrations of the two species and the boundary conditions that can be either open or periodic. As output, we obtain the distance vector from each molecule to its closest nanoparticle (NP). This follows from a key assumption: at low densities each molecule interacts strongly with only one NP.

We use these distances, together with the SIE results, to compute various statistics about the system, such as mean QY enhancement and mean radiative rate enhancement. With these tensors and the molecular orientations, we can calculate the mean increase in quantum yield for any intrinsic quantum yield without rerunning the simulation.

2.1 Electromagnetic factor-tensor calculation

To model the systems of interest we require the radiative enhancement factor F_{rad} and the quenching factor F_q of a fluorescent molecule near a NP. Because the molecules in the ensembles are randomly oriented, we also need a way to obtain these factors for any dipole orientation without rerunning the expensive SIE simulation.

We choose to model the molecule as an electric dipole situated less than a wavelength away from the nanoparticle. This lets us express the factors as power ratios[12]:

$$F_{rad} = \frac{P_{rad}}{P_{dip}}, \qquad F_q = \frac{P_{abs}}{P_{dip}}.$$

The radiated power is the sum of the scattered power P_{sca} and the incident power P_{inc}. These two can be computed by integrating the far-field Poynting flux over a large sphere[13]:

$$P_{sca} = \frac{1}{2Z} \int dA \, |\mathbf{E}|^2$$
$$P_{inc} = \frac{1}{2Z} \int dA \, |\mathbf{E}|^2.$$

The electric field generated by a unit dipole is related to the Green function by

$$\mathbf{E}(\mathbf{r}) = \mu_0 \omega^2 \overleftrightarrow{G}(\mathbf{r}, \mathbf{r}_0) \, \mathbf{p}$$

where $\mathbf{p}$ is the dipole moment, $\mathbf{r_0}$ is the position of the dipole and $\mathbf{r}$ is the point and which we evaluate the electric field.

Substituting this relation yields

$$P_{sca} = \mathbf{p}^* \left(\frac{1}{2Z} \int dA\, \mu_0^2 \omega^4\, G^* G \right) \mathbf{p} = \mathbf{p}^* \mathbf{A}_{sca} \mathbf{p},$$
$$P_{inc} = \mathbf{p}^* \mathbf{A}_{inc} \mathbf{p}.$$

Evaluating the integral in parentheses gives a rank-2 tensor that can be contracted with any dipole orientation to obtain the scattered power.

In a similar way we can show that the absorbed power can be expressed as a tensor contraction starting from the equation

$$P_{abs} = \frac{1}{2} \int_V \mathrm{Re}\big[\sigma(\mathbf{r})\, |\mathbf{E}(\mathbf{r})|^2\big]\, dV.$$

Collecting terms, we define three tensors A_{sca} and A_{abs} such that

$$\mathbf{n} \cdot A_{sca} \cdot \mathbf{n} = P_{sca}, \quad \mathbf{n} \cdot A_{inc} \cdot \mathbf{n} = P_{dip}, \quad \mathbf{n} \cdot A_{abs} \cdot \mathbf{n} = P_{abs},$$

where $\mathbf{n}$ is the unit dipole orientation.

Using these tensors we can also compute the increase in the quantum yield for each molecule:

$$q = \frac{F_{rad}}{F_{rad} + Fq + \frac{1}{q^o} - 1}.$$

2.2 Choice of SIE evaluation points

Thanks to spherical symmetry, a sphere requires evaluation only along a line through its center. A nanorod has only azimuthal symmetry, which removes one dimension; we therefore evaluate the tensors on a two-dimensional grid around the NP. Because the fields vary most rapidly near the nanorod, we place grid points more densely there and more sparsely farther away. Figure 1 shows the chosen evaluation points for the nanorod obtained using a modified Poisson disk sampling algorithm[14]. Using these data-points, we apply a 2-D linear interpolator to get the value at any point around the nanorod.

2.3 Ensemble simulation

To obtain a realistic distribution of molecules and nanoparticles we use a Monte Carlo algorithm. The implementation is split between a C++ `pybind11` core and a Python wrapper. The C++ section releases the global interpreter lock (GIL), allowing the code to run in parallel using Python threads.

We begin by populating the domain with the desired NPs, which are partitioned into a cell list[15] data structure that enables constant-time neighbor checks. NPs are inserted one at a time with a position that is uniformly

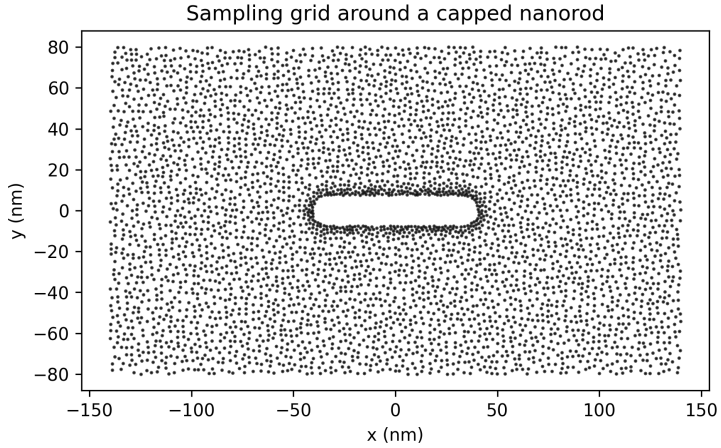

Figure 1: Evaluation points around the 66.0 nm × 7.5 nm nanorod

sampled on all three axes of the domain; if a proposed position collides with an existing NP we reject it and resample. After reaching the target NP density, we use the same rejection-sampling procedure to place molecules in a uniform spatial distribution while assigning each one a random orientation. Collisions are avoided only with NPs, as intermolecular collisions are neglected because the molecules are much smaller than the NPs.

Next, we rebuild the cell list with cell sizes equal to the chosen interaction distance. For each molecule we search the 27 neighboring cells, find the nearest NP and call a user-defined Python function to sample the desired information from the ensemble.

3 Results

To maximize the quantum-yield enhancement we first identify the plasmonic resonances of the nanoparticles under study. We therefore calculate the scattered power under plane-wave illumination for each geometry over a wide spectral range using the surface integral equation (SIE) solver.

For a spherical gold nanoparticle with radius $R = 20\,\text{nm}$, the plasmon resonance appears at $\lambda = 515.5\,\text{nm}$. A gold nanorod of length $L = 66\,\text{nm}$ and hemispherical-cap radius $R = 7.5\,\text{nm}$ exhibits a longitudinal resonance at $\lambda = 780.0\,\text{nm}$. These results are summarized in Figure 2.

3.1 Nanosphere measurements

For a nanosphere we compute the factors along a line perpendicular to its surface, from 0 nm to 250 nm away from the edge. The results are shown in

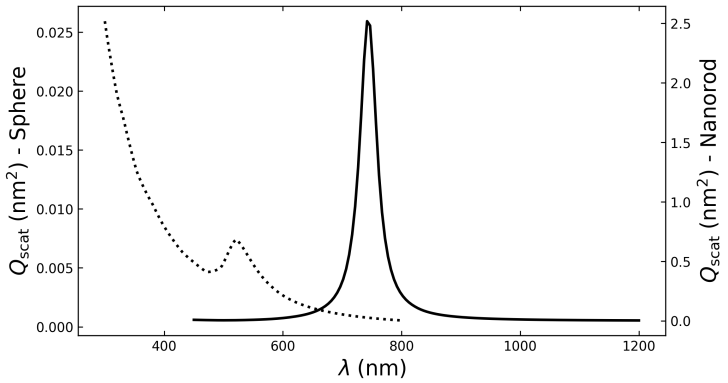

Figure 2: Scattering cross-sections of a 20 nm Au nanosphere and a 66 nm × 7.5 nm capped Au nanorod under plane-wave illumination.

Figure 3; there is almost no radiative enhancement for a tangentially oriented dipole, whereas the quenching is similar for both orientations.

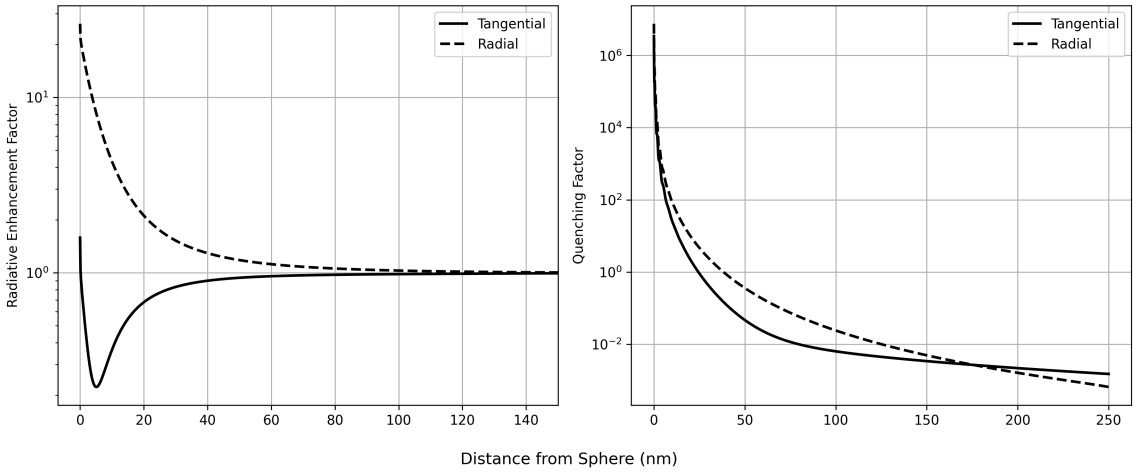

Figure 3: Radiative enhancement and quenching for a gold spherical nanoparticle.

Using these factor tensors we compute the change in quantum yield for different intrinsic quantum yields q_0 and for both dipole orientations. Figure 4 shows that a tangentially oriented molecule gains no quantum-yield enhancement for any q_0. A radial dipole, however, exhibits some enhancement when $q_0 < 0.1$.

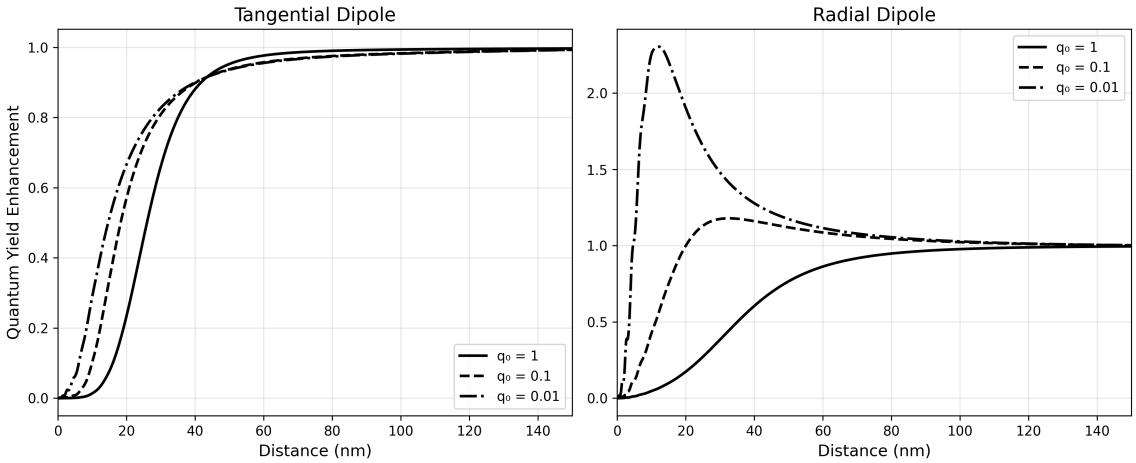

Figure 4: Modification of the quantum yield of the molecules.

3.2 Molecule–nanosphere distribution

Running a Monte Carlo simulation in a $1\,\mu m \times 1\,\mu m \times 1\,\mu m$ cubic box with periodic boundary conditions with a molecule concentration of $1 \times 10^4\,\mu m^{-3}$ and variable nanoparticle number density yields the distributions in Figure 5. As the nanoparticle density increases, the distribution narrows and the average distance decreases, indicating that significant molecule–nanoparticle interactions require a high NP density. It is important to that for high NP concentrations it may be insufficient to assume that each molecule only interacts with one nanoparticle which may impact the validity of the results in that range, requiring further study.

Figure 6 shows that the quantum yield is enhanced only for particles with $q_0 < 0.01$, and the enhancement increases with nanoparticle density. We do not consider here the effects of increasing the molecule concentration, since there is no interaction between them. This means that for every molecule, we sample from the same distribution, and an increase in the molecule density will only decrease the variance of the mean of the QY enhancement.

3.3 Nanorod measurements

Because a nanorod has only azimuthal symmetry, we evaluate the factor tensor on a two-dimensional plane around the nanorod. After running the SIE simulation we linearly interpolate the results, obtaining values throughout the surrounding space. Figure 7 summarizes the factors for different dipole orientations. We see that the field pattern rotates together with the orientation of the dipole.

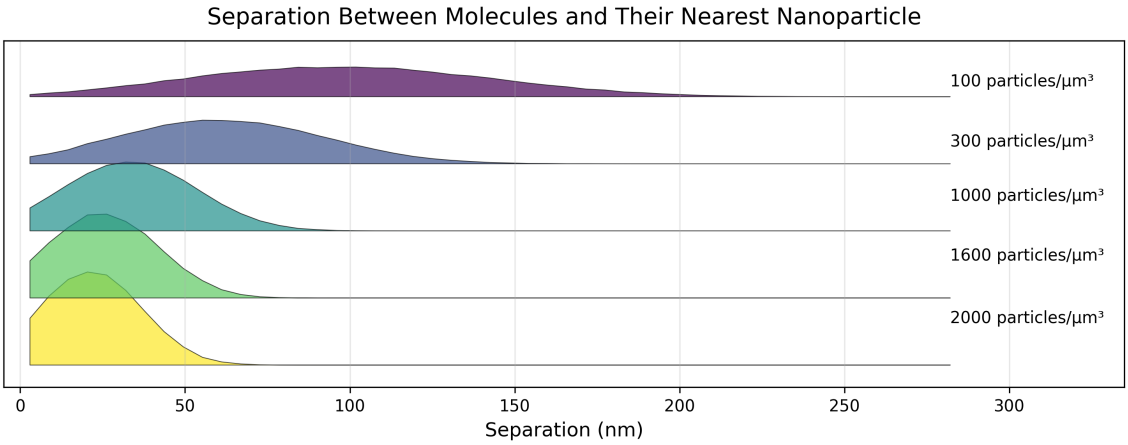

Figure 5: Distribution of the distance from a molecule to its nearest nanosphere at different nanoparticle number densities.

Using what we have computed we can get a picture of the quantum yield enhancement of molecules around the nanorod. This is illustrated in Figure 8, where we see a similar behavior to the enhancement factors. Above and below the nanorod the enhancement is only significant up to 50 nm. It is interesting to note that there is almost no enhancement at the tips of the nanorod.

3.4 Molecule-nanorod distribution

We use a Monte Carlo simulation to generate ensembles of molecules and nanorods at different densities. Figure 9 shows the molecular positions in the reference frame of the nearest nanorod. As with the nanosphere ensembles, increasing nanoparticle density brings the molecules closer to the nanorod on average. Most molecules cluster above the nanorod sides and are centered laterally.

To see how the average quantum yield changes based on the concentrations, we do a sweep of the nanorod density from $100\,\mu m^{-3}$ to $4000\,\mu m^{-3}$. This is shown in Figure 10, where we see that for $q_0 < 0.01$ the average enhancement grows slower than linearly with the density of the nanorods.

4 Discussion and Conclusion

The numerical results presented above suggest that a high concentration of nanoparticles is needed to achieve significant quantum yield enhancement, for both nanosphere and nanorod ensembles. We see that nanorods are more promising, achieving around 12 times the enhancement of the nanosphere

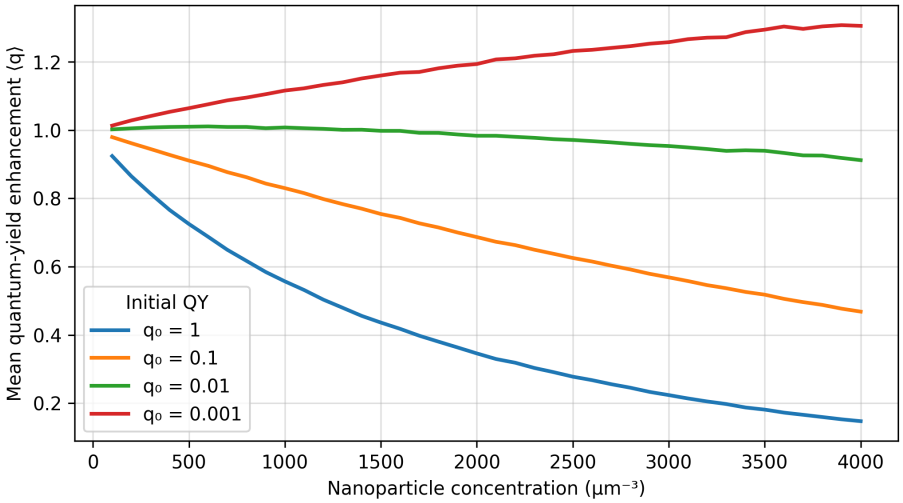

Figure 6: Average quantum-yield modification versus nanoparticle density.

solution at concentrations of $4000\,\mu m^{-3}$, for an intrinsic quantum yield $q_0 = 0.001$.

Based on the trends that appear in Figure 6 and Figure 10, we see that the mean quantum yield enhancement increases with the nanoparticle concentration. In this high-concentration regime, more work needs to be done to ensure the validity of our approximation and quantify the error of our approximations. At these concentrations molecules are more likely to interact with multiple NPs at the same time, which invalidates our single-interaction assumption.

A major contributing factor to the loss of quantum yield enhancement is the orientation of the molecules. For a nanosphere, a tangential orientation of the dipole moment provides no enhancement at any distance, meaning that only half of the molecules on average contribute to the increase in the mean QY. For a nanorod, both molecules oriented along the principal axis and ones that are radially oriented contribute to the QY. However, molecules that are oriented tangentially do not, lowering the overall enhancement. This suggests that an avenue for improving the QY could be by finding ways of controlling the orientations of the molecules and NPs, or by searching for NP geometries that offer a good enhancement regardless of the orientation of the molecule.

In summary, the present simulations underline the stringent conditions required for meaningful quantum-yield enhancement in molecule–nanoparticle mixtures; although the surface-integral tensor approach captures the underlying mechanism accurately, practical realization will likely demand either strict control over molecular orientation or nanoparticle architectures that provide stronger and more spatially accessible near-field enhancements.

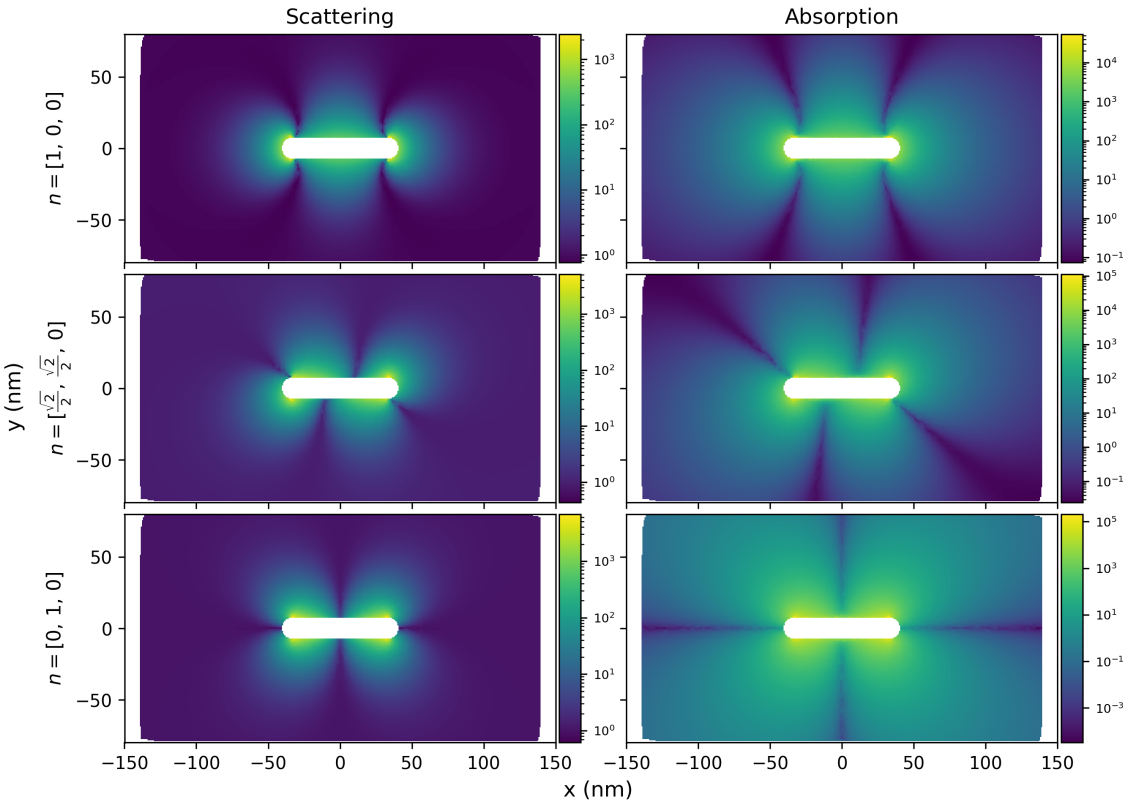

Figure 7: Radiative enhancement and quenching factors around a gold nanorod for various dipole orientations.

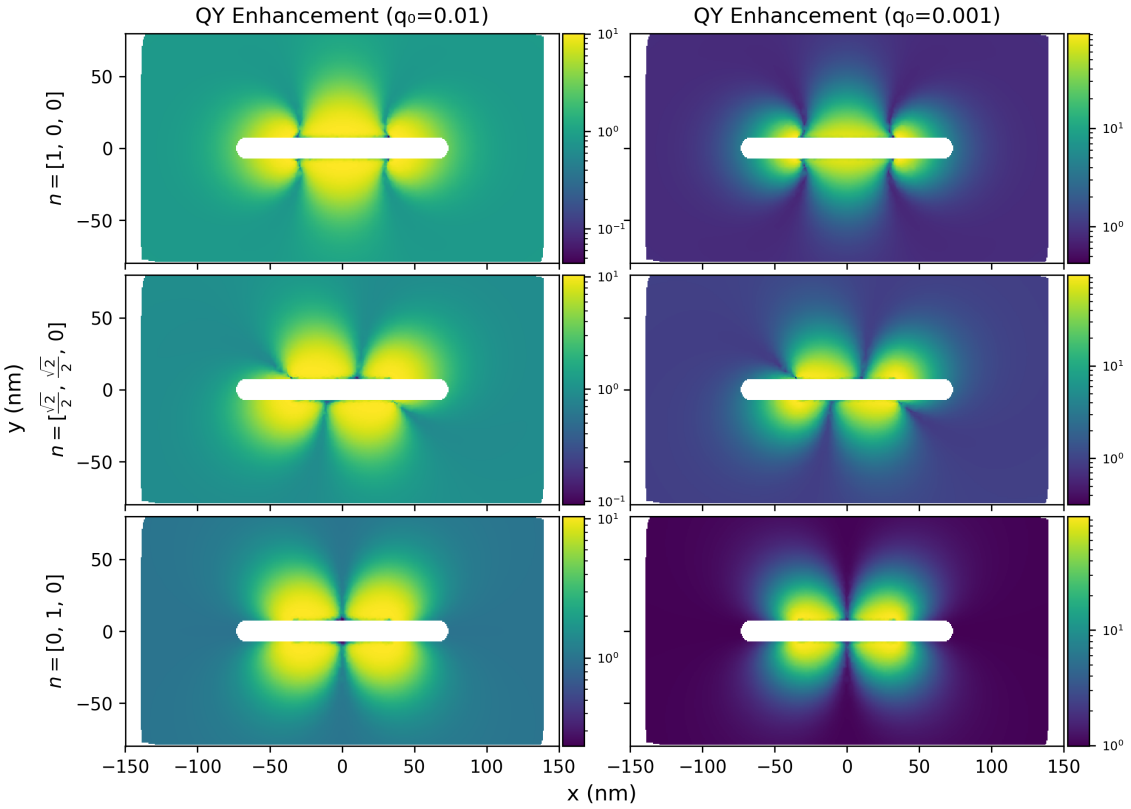

Figure 8: Quantum yield enhancement around the nanorod for different molecule orientations

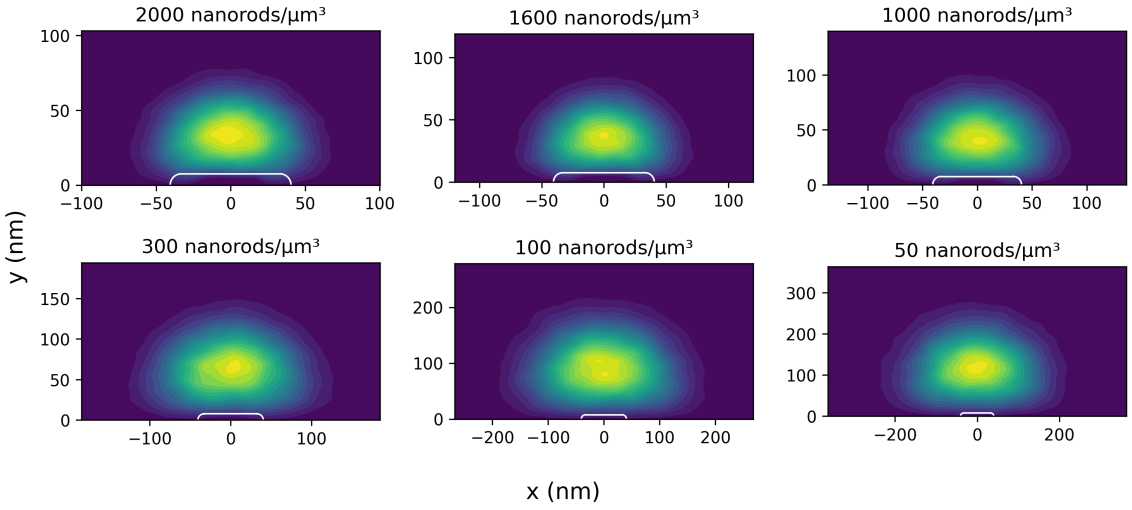

Figure 9: Spatial distribution of molecules relative to the nearest nanorod at different nanoparticle densities.

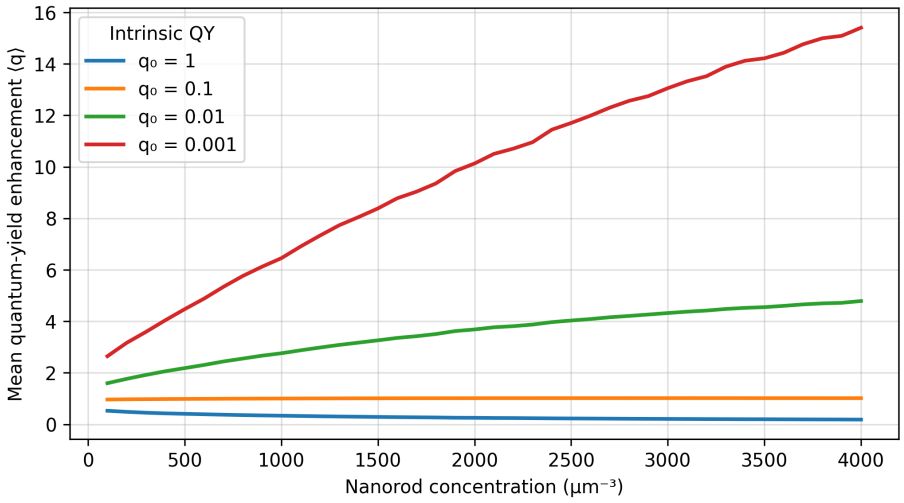

Figure 10: Average quantum yield of the system as a function of nanorod density

References

[1] Kasey J. Russell et al. "Large spontaneous emission enhancement in plasmonic nanocavities". In: *Nature Photonics* 6.7 (2012), pp. 459–462. DOI: 10.1038/nphoton.2012.112.

[2] Lavinia Rogobete et al. "Design of plasmonic nanoantennae for enhancing spontaneous emission". In: *Optics Letters* 32.12 (2007), pp. 1623–1625. DOI: 10.1364/OL.32.001623.

[3] Pascal Anger, Palash Bharadwaj, and Lukas Novotny. "Enhancement and quenching of single-molecule fluorescence". In: *Physical Review Letters* 96.11 (2006), p. 113002. DOI: 10.1103/PhysRevLett.96.113002.

[4] Guillermo P. Acuña et al. "Fluorescence enhancement at docking sites of DNA-directed self-assembled nanoantennas". In: *Science* 338.6106 (2012), pp. 506–510. DOI: 10.1126/science.1228638.

[5] Emiliano Cortés et al. "Plasmonic nanoprobes for stimulated emission depletion nanoscopy". In: *ACS Nano* 10.11 (2016), pp. 10454–10461. DOI: 10.1021/acsnano.6b06361.

[6] Na-Yeong Kim, Sang-Hyun Hong, and Jang-Won et al. Kang. "Localized surface plasmon-enhanced green quantum dot light-emitting diodes using gold nanoparticles". In: *RSC Advances* 5.25 (2015), pp. 19624–19629. DOI: 10.1039/C4RA15585H.

[7] Alberto G. Curto, Giorgio Volpe, and Tim H. et al. Taminiau. "Unidirectional emission of a quantum dot coupled to a nanoantenna". In: *Science* 329.5994 (2010), pp. 930–933. DOI: 10.1126/science.1191922.

[8] Thang B. Hoang, Gleb M. Akselrod, and Christos et al. Argyropoulos. "Ultrafast spontaneous emission source using plasmonic nanoantennas". In: *Nature Communications* 6 (2015), p. 7788. DOI: 10.1038/ncomms8788.

[9] Stephan Link and Mostafa A. El-Sayed. "Spectral Properties and Relaxation Dynamics of Surface Plasmon Electronic Oscillations in Gold and Silver Nanodots and Nanorods". In: *Journal of Physical Chemistry B* 103 (1999), pp. 8410–8426. DOI: 10.1021/jp9917648.

[10] Anton M. Kern and Olivier J. F. Martin. "Surface integral formulation for 3D simulations of plasmonic and high-permittivity nanostructures". In: *Journal of the Optical Society of America A* 26.4 (2009), pp. 732–740.

[11] T. V. Raziman et al. "Accuracy of surface integral equation matrix elements in plasmonic calculations". In: *Journal of the Optical Society of America B* 32.3 (2015), pp. 485–492.

[12] Lukas Novotny and Bert Hecht. *Principles of Nano-Optics*. 2nd. Cambridge, UK: Cambridge University Press, 2012. ISBN: 978-1107005461.

[13] Andreas M. Kern et al. “Enhanced single-molecule spectroscopy in highly confined optical fields: from /2-Fabry–Pérot resonators to plasmonic nano-antennas”. In: *Chemical Society Reviews* 43.4 (2014), pp. 1263–1286. DOI: 10.1039/C3CS60357A. URL: https://doi.org/10.1039/C3CS60357A.

[14] Robert L. Cook. “Stochastic Sampling in Computer Graphics”. In: *ACM Transactions on Graphics* 5.1 (1986), pp. 51–72.

[15] Daan Frenkel and Berend Smit. *Understanding Molecular Simulation: From Algorithms to Applications*. 2nd. Vol. 1. Computational Science Series. San Diego: Academic Press, 2002. ISBN: 0122673514.